Eur. Phys. J. A **14**, 225–238 (2002)
DOI 10.1140/epja/i2001-10122-3

THE EUROPEAN PHYSICAL JOURNAL A

Irreducible pionic effects in nucleon-deuteron scattering below 20 MeV

L. Canton[1,a], W. Schadow[2,b], and J. Haidenbauer[3]

[1] Istituto Nazionale di Fisica Nucleare, Sezione di Padova, Via F. Marzolo 8, Padova I-35131, Italy
[2] Dipartimento di Fisica dell'Università di Padova, Via F. Marzolo 8, Padova I-35131, Italy
[3] Forschungszentrum Jülich, IKP, D-52425 Jülich, Germany

Received: 21 November 2001 / Revised version: 22 January 2002
Communicated by A. Molinari

Abstract. The consequences of a recently introduced irreducible pionic effect in low-energy nucleon-deuteron scattering are analyzed. Differential cross-sections, nucleon (vector) and deuteron (vector and tensor) analyzing powers, and four different polarization transfer coefficients are considered. This $3NF$-like effect is generated by the pion exchange diagram in presence of a two-nucleon correlation and is partially cancelled by meson retardation contributions. Indications are provided that such type of effects are capable to selectively increase the vector (nucleon and deuteron) analyzing powers, while in the considered energy range they are almost negligible on the differential cross-sections. These indications, observed with different realistic nucleon-nucleon interactions, provide additional evidences that such $3NF$-like effects have indeed the potential for solving the puzzle of the vector analyzing powers. Smaller but non-negligible effects are observed for the other spin observables. In some cases, we find that the modifications introduced by such pionic effects on these spin observables (other than the vector analyzing powers) are significant and interesting and could be observed by experiments.

PACS. 24.70.+s Polarization phenomena in reactions – 21.30.Cb Nuclear forces in vacuum – 25.10.+s Nuclear reactions involving few-nucleon systems – 25.40.Dn Elastic neutron scattering

1 Introduction

As is well known, nuclear potentials (two-, three-, and many-body) are generated when the relevant non-nucleonic degrees of freedom (isobars and the force-mediating mesons) are eliminated from the field-theoretic Fock space with the aim to treat nuclear dynamics within the restricted, purely nucleonic, Hilbert space.

One could view this fact also in the following way: instead of solving the full nuclear problem in one single step in terms of all its effective constituents (*e.g.*, nucleons, isobars, and mesons), one separates for convenience the problem into two steps. First, a model solution of the field-theoretic problem is sought in the enlarged space where there is, in every intermediate state, at least a meson (or an isobar). This produces a set of subamplitudes which can be identified as nuclear potentials. Then, as result of this first step, the nuclear forces can be used as input for the calculation of the subsequent task, represented by the non-relativistic quantum-mechanical solution of the nuclear dynamics within the purely nucleonic Hilbert space.

Obviously, the first step can only be determined in some approximate way, since the problem represents, in terms of its effective field-theoretic constituents, an extremely complicated task. Thus, it has been inevitable that a variety of strategies for determining the nuclear potentials in different model spaces have been developed. For two-nucleon potentials, many indeterminations implicit in all approaches can be constrained up to a high level of accuracy by comparison with the phenomenological NN phase shifts, but the situation is much less developed for three-nucleon potentials. (And still in its infancy for contributions involving more than three nucleons, although general dimensional arguments based on power-counting schemes predict that the many-nucleon contributions rapidly decrease toward zero with increasing number of nucleons.)

Considerations about three-nucleon potentials appeared soon to be strongly dependent on the theoretical strategies employed to reduce the enlarged space involving mesons and baryons into the more tractable purely fermionic/nucleonic space. A paradigmatic example is discussed in an article (ref. [1]) with this remarkable title: *The three-nucleon force is not made by nature.* A more technical review can be found in ref. [2]. These two articles

[a] e-mail: `luciano.canton@pd.infn.it`
[b] *Permanent address*: Cap Gemini Ernst & Young, Hamborner Str. 55, 40472 Düsseldorf, Germany.

focus attention in particular on the dynamical aspects of the Δ isobar. On the other hand, there are ambiguities in the definition of a three-nucleon force ($3NF$) connected, *e.g.*, with the treatment of mesonic-retardation effects, although there are consistency conditions that relate the different definitions to each other. As observed in ref. [3], these ambiguities arise because the (three-nucleon) potential is an unphysical theoretical object, obtained from a subamplitude according to a set of prescriptions.

The first non-nucleonic ingredient that plays a crucial role for nuclear systems is the pion, and it is natural to aim at a theoretical formulation that couples dynamically this meson to the nucleonic degrees of freedom. Such a formulation would then provide a combined description of nuclear systems at low and intermediate energies. Pions are produced indeed and observed by experiments at intermediate energies and their dynamical role in these nuclear systems can hardly be ignored.

With two-nucleon systems, various approaches to include the effects of a dynamical pion in a non-perturbative fashion have been developed and analyzed [4], and many theoretical problems like relativistic aspects, or the proper treatment of the nucleon renormalization effects, or finally the consistent treatment of meson exchange diagrams related by different time orderings, have been extensively discussed [5]. Not all these problems have been solved in a systematic manner since these πNN approaches aim to include just one dynamical pion in the theory, thus ruling out more complex situations with multipionic intermediate states. Stated in other words, these techniques allow to include one single dynamical pion in the $2N$ system, but then one has to face the conceptual problems arising because the states with more than one pion at the same time are ruled out from the dynamical equations. Still, in spite of these problems, the generalization of such type of approaches to the three-nucleon system allows to reveal possible new dynamical aspects of the pion that cannot be observed by freezing out from the very beginning *all* mesonic degrees of freedom, into instantaneous meson exchange potentials.

The dynamical equations for the coupled NN-πNN problem have been generalized to the $3N$ system in ref. [6]. The method is based on the rigorous Yakubovski-Grassberger-Sandhas [7,8] four-body theory, extended to the πNNN system with an absorbable pion. Previously, this problem has been analyzed with few-body techniques for quite a few years [9–11]. The solution of the resulting set of 21×21 coupled equations represents a formidable task, and for practical reasons an approximation scheme to reduce the complexity of the original equations to an approximated but more tractable form has been developed [12]. The approximation scheme builds up the complete dynamical solution starting from the zeroth-order solution, given by the standard quantum-mechanical Alt-Grassberger-Sandhas (AGS) equation [13]. The theoretical strategy that emerges from this approximation scheme consists in treating the normal $2N$ correlations "exactly" via Faddeev-like methods, while the additional mesonic aspects which cannot be adequately described by a conventional $2N$ potential have to be incorporated directly into the dynamical equation as corrections (*i.e.* through an underlying perturbative-iterative expansion). This is consistent with the findings of the approaches based on chiral perturbation theory (ChPT) which predict that $3NF$ effects are small [14].

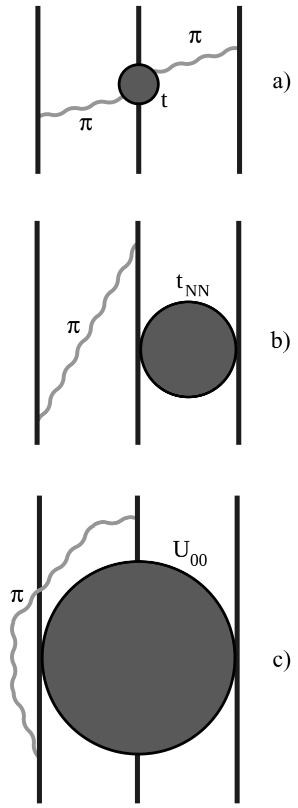

Fig. 1. $3NF$-type diagrams appearing at the lowest order from the treatment of the coupled π-NNN system.

To the lowest order, the approximation scheme ends up with three different types of irreducible $3NF$ diagrams which have to be incorporated in the dynamical equations according to the prescriptions given in ref. [12]. These diagrams are shown in fig. 1. Clearly, all three types of diagrams are related to specific aspects of the pion dynamics which cannot be incorporated in the description of a purely nucleonic system interacting through a pair-wise potential.

Amongst the three types of diagrams, one can easily recognize the extensively studied 2π-$3NF$ diagram, labeled a) in the figure. This diagram has led to various models of $3N$ potential amongst which we recall two historical representations, Tucson-Melbourne [15] and Brazil [16]. These potentials use the πNN vertices and the off-shell extrapolated πN amplitudes as inputs. It is important to observe that in the construction of these potentials certain diagrams have to be subtracted explicitly, to avoid double countings. The other two types of diagrams that emerge at the lowest order involve the intermediate formation of a $2N$ correlation while one pion is being exchanged, and finally the intermediate formation of a $3N$ correlation, during the exchange process (diagrams b) and c)), respectively, in fig. 1). The last type of diagram involves the connected part of the $3N \to 3N$ amplitude, denoted U_{00} in the figure, and has been discussed in the previous literature only occasionally [17], and to our knowledge, its effect has not yet been estimated quantitatively in realistic situations, although its relevance might not be so important because the probability that a full $3N$ correlation is formed during the meson exchange process is expected to be small.

The diagram 1b), involving the full $2N$ t matrix during a pion exchange process, has been discussed in ref. [18]. The consequent appearance of an irreducible $3N$ operator with tensor-like structure has also been observed therein (see also refs. [19,20]). In the construction of this operator, certain classes of subdiagrams have to be subtracted, because of the presence of a cancellation effect which has been observed in the literature quite a few years ago [21,22]. The connection between the nature of these cancellations and their implications to the ChPT approach has been discussed in ref. [3]. A similar cancellation effect has been also observed —in leading order— in effective nuclear forces based on chiral Lagrangians and constructed with the method of unitary transformation [23]. As has been discussed in refs. [18–20], however, such subtraction leads to a cancellation effect which is only partial if the original $3NF$ diagram has been derived within a dynamical approach which leads to an energy-dependent $3NF$-like operator, and where the meson propagates for a sufficiently extended time to allow the intermediate formation of a correlated $2N$ pair. That might correspond to the inclusion of a series of non-vanishing higher-order terms in the chiral expansion. In the standard approach which uses instantaneous two- and three-nucleon interactions, the freezing out of the mesonic degrees of freedom does not contemplate the occurrence of such a $3NF$ effect.

In ref. [19], the consequences of considering this type of one-pion exchange $3NF$ diagram (OPE-$3NF$) in the $3N$ equation have been studied. It was shown that this diagram has the potential to modify considerably the vector analyzing powers A_y without affecting appreciably the differential cross-section, and could therefore solve the long standing puzzle of the vector analyzing powers in nucleon-deuteron scattering below 30 MeV. On the other hand, other alternative explanations have been suggested in the literature. Effective three-nucleon potentials constructed with a combination of short-range and pion-range terms have been considered first under the point of view of the meson exchange picture [24], and later reconsidered under the framework of chiral perturbation theory [25], since a non-negligible role for these terms is predicted. A phenomenological spin-orbit three-body operator has also been introduced [26] in order to improve the vector analyzing powers. Another explanation [27] advocates the Brown-Rho scaling-with-density hypothesis [28] in the three-nucleon system. Because of this scaling, the $2N$ potential has been modified specifically in the triplet P waves by reducing the scalar- and vector-meson masses to approximately 95% of their free-space value, thereby enhancing the spin-orbit term of the density-dependent $2N$ potential with respect to free space. This selective dependence of the A_y puzzle on the triplet P waves of the $2N$ force suggested also that modern phase-shift analysis might have not yet been settled to the correct parameters for these states in the low-energy domain [29]. But it has also been argued [30] that the required changes of the free-space $2N$ potential have to be exceedingly drastic for the one-pion exchange contribution, which on the contrary is well established.

In the present paper, we have extended the study of ref. [19] about the irreducible pionic effect implied by the OPE-$3NF$ diagram by considering such an effect with three different $2N$ potentials. In all cases we were able to demonstrate that this irreducible pionic effect has the potential to solve the puzzle for the low-energy vector analyzing powers with negligible effects for the differential cross-sections and minor effects for the other spin observables. We have also widened the comparison with experimental data by including differential cross-sections, vector and tensor analyzing powers, and spin transfer coefficients at various energies below 20 MeV.

The basic structure of the OPE-$3NF$ diagram is recalled in sect. 2. Comparison between theory and experiments is made in sect. 3. Conclusions are derived in sect. 4.

2 Theory

Following refs. [6,12,18,19], we have incorporated directly into the Faddeev-AGS three-nucleon equation the irreducible effects generated by the one-pion exchange mechanism in the presence of a nucleon-nucleon correlation. The detailed expression has been discussed previously in ref. [18]. It is reported here for convenience:

$$
\begin{aligned}
V_3^{3N}(\mathbf{p},\mathbf{q},\mathbf{p}',\mathbf{q}';E) &= \frac{f^2_{\pi NN}(Q)}{m_\pi^2}\frac{1}{(2\pi)^3} \\
&\times\left[\frac{(\boldsymbol{\sigma_1}\cdot\mathbf{Q})(\boldsymbol{\sigma_3}\cdot\mathbf{Q})(\boldsymbol{\tau_1}\cdot\boldsymbol{\tau_3})+(\boldsymbol{\sigma_2}\cdot\mathbf{Q})(\boldsymbol{\sigma_3}\cdot\mathbf{Q})(\boldsymbol{\tau_2}\cdot\boldsymbol{\tau_3})}{\omega_\pi^2}\right] \\
&\times\frac{\tilde{t}_{12}(\mathbf{p},\mathbf{p}';E-\frac{q^2}{2\nu}-m_\pi)}{2m_\pi} \\
&+\frac{f^2_{\pi NN}(Q)}{m_\pi^2}\frac{1}{(2\pi)^3}\frac{\tilde{t}_{12}(\mathbf{p},\mathbf{p}';E-\frac{q'^2}{2\nu}-m_\pi)}{2m_\pi} \\
&\times\left[\frac{(\boldsymbol{\sigma_1}\cdot\mathbf{Q})(\boldsymbol{\sigma_3}\cdot\mathbf{Q})(\boldsymbol{\tau_1}\cdot\boldsymbol{\tau_3})+(\boldsymbol{\sigma_2}\cdot\mathbf{Q})(\boldsymbol{\sigma_3}\cdot\mathbf{Q})(\boldsymbol{\tau_2}\cdot\boldsymbol{\tau_3})}{\omega_\pi^2}\right]. \quad (1)
\end{aligned}
$$

The momenta $\mathbf{p}, \mathbf{q}$ represent respectively the Jacobi coordinates of the pair "12", and spectator "3", while E is the $3N$ energy. The pion-nucleon coupling constant is selected by the underlying $2N$ potential that is considered; for instance, for the Paris and Bonn potentials, we have used the "traditional" value $f^2_{\pi NN}/(4\pi) = 0.078$, while for the newer CD Bonn potential [31] we have consistently used the more recent determinations by the Nijmegen [32] and VPI [33] group. The same considerations have been applied for the pion-nucleon form factor, since we have employed the same standard functions (and also with the same parameters) that have been employed at the level of the $2N$ potentials

$$f_{\pi NN}(Q) = f_{\pi NN} \frac{\Lambda_\pi^2 - m_\pi^2}{\Lambda_\pi^2 + Q^2}\,. \qquad (2)$$

The transferred momentum $\mathbf{Q} = \mathbf{q}' - \mathbf{q}$ enters also in $\omega_\pi = \sqrt{m_\pi^2 + Q^2}$. $\tilde{t}_{ij}$ denotes the subtracted t matrix between nucleons 1 and 2, defined according to the prescription

$$\tilde{t}_{12}(\mathbf{p}, \mathbf{p}'; Z) = c(E)\, t_{12}(\mathbf{p}, \mathbf{p}'; Z) - v_{12}(\mathbf{p}, \mathbf{p}')\,. \qquad (3)$$

We have considered in addition another possible type of subtraction

$$\tilde{t}_{12}(\mathbf{p}, \mathbf{p}'; Z) = c(E)\, t_{12}(\mathbf{p}, \mathbf{p}'; Z) - t_{12}(\mathbf{p}, \mathbf{p}'; -\tilde{\Lambda})\,, \qquad (4)$$

where the subtraction parameter $\tilde{\Lambda}$ has been fixed around 1.5 GeV. Other details can be found in refs.[18,19]. The factor $c(Z)$ is an adjustable parameter and serves to control the cancellation between the two terms. Ideally, this factor should be approximately one if the $2N$ t matrix could be reliably extrapolated off-shell down to $Z \simeq -160$ MeV. However, the existing $2N$ potentials cannot guarantee the extrapolation at such negative energies. Moreover, additional approximations and simplifications entered in the determination of the expression for V_3^{3N}, as discussed in ref. [18,19]. For these reasons, we introduced $c(Z)$ as adjustable parameter, with the constrain that at higher energies in nd scattering, this factor should move towards one, because the $2N$ t matrix entering in V_3^{3N} is then calculated at energies higher than $\simeq -160$ MeV, that is, less far off-shell. The use of the second type of subtraction, eq. (4), has been introduced in the case of the Paris potential because this potential is not OBE like (one-boson exchange). In this case, the subtraction of the meson-exchange diagrams involved in the cancellation is therefore not feasible with eq. (3). On the other hand, eq. (4) tends to enhance the cancellation effects with respect to eq. (3), and therefore it is to be expected that the parameter governing the cancellation in eq. (4) has to compensate this effect.

The irreducible pionic effect described by eq. (1) can be incorporated in the scattering equation in a convenient way if the $2N$ input potential is of finite rank. For a rank-one (separable) case, the $2N$ t matrix takes the expression $t = |g_1\rangle \tau \langle g_1|$, and the (anti)symmetrized AGS equation can be reinterpreted as an effective two-body multichannel integral equation in one intercluster momentum variable,

$$X_{11} = Z_{11} + Z_{11} \tau X_{11}, \qquad (5)$$

with the driving term calculated as follows:

$$Z_{11} = \langle g_1 | G_0 P | g_1 \rangle + \langle g_1 | G_0 V_1^{3N} G_0 | g_1 \rangle\,. \qquad (6)$$

The first contribution represents the standard AGS driving term, with G_0 and P being the free Green's function and the cyclic/anticyclic permutator, respectively, while the second expression takes into account the effects of the irreducible $3N$ diagram discussed above. The procedure is consistent with the formalism developed in ref. [12] to include irreducible pionic effects as corrections in the Faddeev-AGS equation. Since the formalism is based on the systematic 4-body approach of ref. [6], it allows to include additional (high-order) classes of irreducible diagrams in subsequent steps.

Table 1. Ranks used in the separable expansion for each $2N$ state and for the various potentials. For the CDB-EST potential in the $^1S_0$ channel, the expansion has been done separately for nn and pn cases.

NN states	P-EST	BB-EST	CDB-EST
$^1S_0$	5	5	5(+5)
$^3S_1$–$^3D_1$	6	6	6
$^3P_0$	5	4	4
$^1P_1$	5	4	4
$^3P_1$	5	4	4
$^1D_2$	5	4	4
$^3D_2$	5	4	4
$^3P_2$–$^3F_2$	5	5	5

Neutron-deuteron scattering observables below 20 MeV have been calculated using the finite-rank representation of realistic nucleon-nucleon potentials, known as P-EST, BB-EST, and CDB-EST potentials [34–36]. These provide accurate representation of the nucleon-nucleon transition matrix for the Paris (P) [37], Bonn-B (BB) [38], and CD-Bonn (CDB) [31] potentials and are based upon the Ernst-Shakin-Thaler (EST) method [39] for generating the finite-rank expressions of the transition matrices and/or potentials. Benchmark calculations [40, 41] for scattering and bound-state regime have demonstrated that with this method it is possible to solve accurately the Faddeev-AGS scattering equations, and to obtain results comparable (with errors of 1% or less) to those obtained from a direct solution of the 2-dimensional Faddeev equations (where the original $2N$ potential is used as input). The results shown in the next section have been calculated with the $2N$ potentials acting in the $j \leq 2$ states, and listed in table 1. For each $2N$ potential and state, the table also reports the rank of the separable expansion used.

Finally, the calculations reported herein have been performed including all $3N$ states with total angular momenta up to $J = 19/2$, for both odd and even parities.

3 Results

We first compare the results of our calculations with experimental data taken with incident neutrons at 3 MeV. At this energy the process is below the deuteron break-up threshold. The experimental data shown in fig. 2 are taken from refs. [42] and [43] for the differential cross-section and the neutron analyzing power, respectively. The figure compares the calculations obtained with the CD-Bonn, Bonn-B, and Paris potentials (dashed, dot-dashed, and dotted lines, respectively) with those obtained when adding consistently the OPE-$3NF$ effect as discussed in the previ-

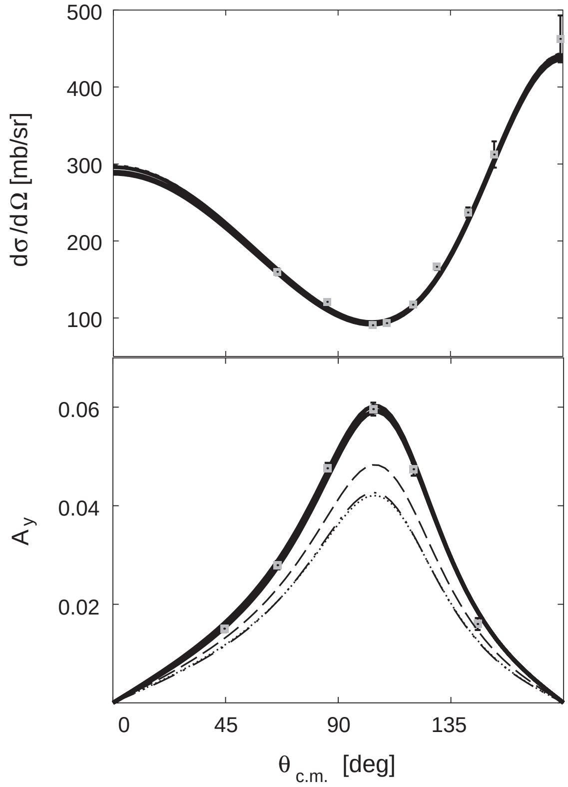

Fig. 2. Differential cross-section and analyzing power for *nd* scattering at 3 MeV (Lab). Calculations with the EST expansion of the Paris potential (dotted line), Bonn-B (dot-dashed) and CD-Bonn (dashed). For each $2N$ potential, the corresponding ranks are given in table 1. The thick solid line contains the resulting modifications introduced by the OPE-$3NF$ effect, for all the three potentials. Data (grey squares) from refs. [42] and [43].

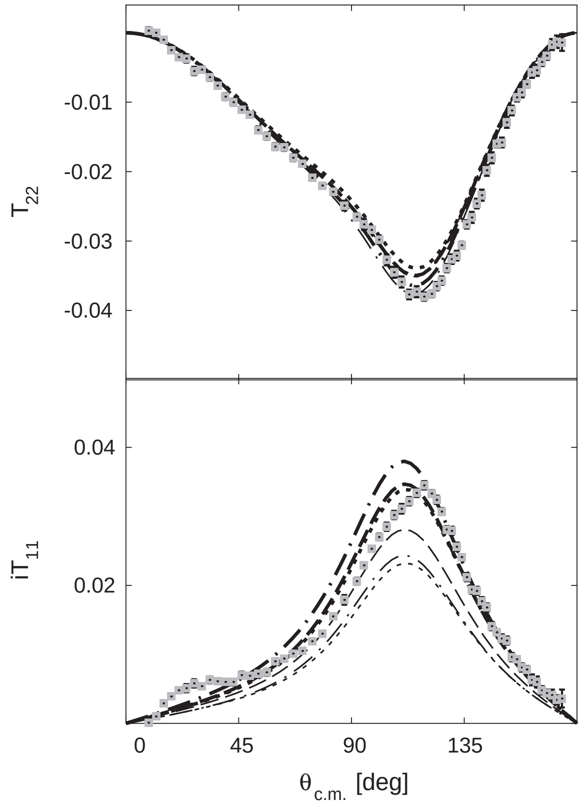

Fig. 3. Deuteron analyzing powers T_{22} (upper panel) and iT_{11} (lower panel) at 3.3 MeV. The three thin lines are calculations with $2N$ potentials only. The corresponding thick lines contain also the OPE-$3NF$ effects. As in the previous figure, dotted, dot-dashed, and dashed lines represent, respectively, the results with Paris, Bonn-B, and CD-Bonn potentials. Data are from ref. [44].

Table 2. Energy dependence of the effective parameter used to govern the cancellation in eq. (3).

E (MeV)	BB-EST	CDB-EST
3.0	0.730	0.58
8.5	0.733	0.60
11.3	0.743	0.63
13.3	0.753	0.65
15.3	0.763	0.67
17.3	0.773	0.69
18.3	0.778	0.70

ous section. By adjusting the parameter in eq. (3) (or in eq. (4) for the Paris potential), we obtain for each considered potential the required modifications for the proper reproduction of the analyzing power without spoiling the description of the differential cross-section. For the Bonn-B and CD-Bonn potentials the actual values of the parameter have been reported in table 2. (For the Paris case the parameter has been set to 0.385.)

For all the three potentials the result of the calculations including the OPE-$3NF$ effect is contained in the thick solid line. For the differential cross-section, there is a very tiny effect or tendency to reduce the differential cross-section in both the forward and backward direction, however, such an effect can hardly be perceived in the figure.

Then, we compare our results with other polarization observables taken at comparable energies. To do so, we consider the complete set of deuteron analyzing power measurements in deuteron-proton scattering at 8 MeV, ref. [44]. The measurements at this energy (for incident deuterons) compares to an equivalent energy of 4 MeV for the case of incident protons. However, we do not include Coulomb corrections in our calculations. As minimal Coulomb correction, we consider exclusively the additional loss of kinetic energy of the proton while approaching the electric field of the deuteron [45]. This loss amounts to about $\simeq 0.7$ MeV and hence we compare the experimental data of ref. [44] with theoretical results obtained with incident neutrons of 3.3 MeV. We observe that the Coulomb slow-down effect has been observed experimentally for A_y and not for the deuteron analyzing powers, since there are no experimental neutron data here. However, a recent calculation [46] (with and without Coulomb force) suggests that the same effect holds also for these observables.

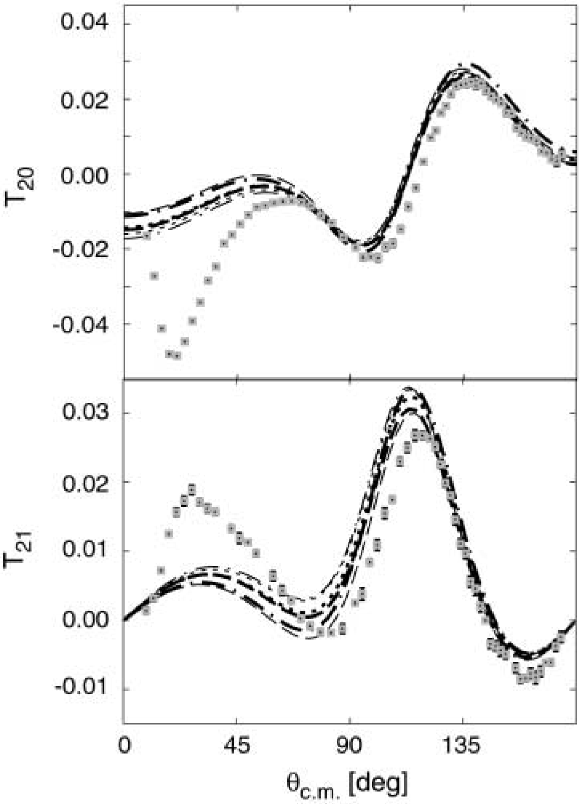

Fig. 4. Same as in fig. 3, but for the T_{20} and T_{21} analyzing powers.

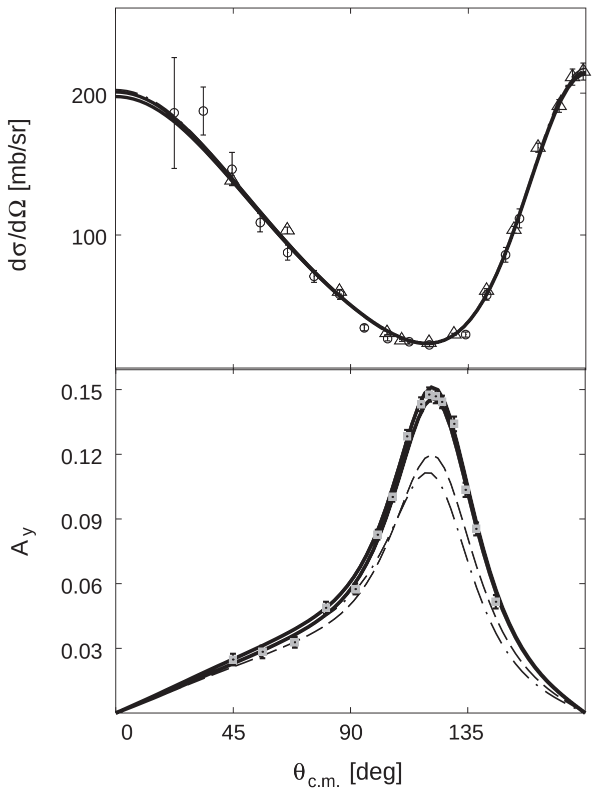

Fig. 5. Same as in fig. 2 but for nd scattering at 8.5 MeV. Data are from refs. [42,47], and [48]. Calculations are for CD-Bonn (dashed line) and Bonn-B (dash-dotted line) potentials. The thick solid line includes the irreducible $3NF$-like effects for both potentials.

The lower panel of fig. 3 considers the deuteron vector analyzing power iT_{11}. Again, we observe that the standard two-nucleon calculations without $3NF$ effects (thin lines) underpredict this observable, while the inclusion of the OPE-$3NF$ effect provides the necessary modifications (thick lines) suggested by the data. Conventions for the lines are the same as in the previous figure, namely, dashed, dot-dashed, and dotted lines, describe calculations with CD-Bonn, Bonn-B, and Paris potentials, respectively. We observe that the inclusion of the OPE-$3NF$ effect for the Bonn-B potential provides the largest effect for iT_{11}, while for the two other potentials the results with the $3NF$ effect are rather similar. This is at variance with respect to the case without $3NF$ effects, where the CD-Bonn potential alone provides a substantially higher iT_{11} with respect to the Paris and Bonn-B cases. Aside from the substantial increase of this observable provided by the OPE-$3NF$ effect, it is difficult to draw any additional conclusions by comparison with experimental data because of the presence of the perturbation introduced by the Coulomb field, which at these energies modifies sensibly the shape of this observable not only in the most forward direction.

The upper panel of fig. 3 considers the deuteron tensor analyzing power, T_{22}. Here the modification introduced by the OPE-$3NF$ are very small and cannot be perceived in the figure, with the exception of the Bonn-B case, where a slight reduction of the dip peaked around 100° can be observed. A similar situation is suggested for the other two deuteron tensor analyzing powers, T_{20} and T_{21}, shown respectively in the upper and lower panel of fig. 4. The introduction of the OPE-$3NF$ effect introduces very slight modifications also in these two observables. Again we observe that with the inclusion of this $3NF$ effect the Paris and CD-Bonn results become more similar than they were before. Also with the Bonn-B potential the modifications are small, although one can clearly perceive for T_{20} that the dip at 100° and the peak in the backward direction are slightly more pronounced. Same situation occurs for the dip at 80° for T_{21}. Comparison with data shows that at these energies and for these observables no definite conclusions can be drawn without an accurate inclusion of the Coulomb field, or without a comparison with accurate measurements involving neutron-deuteron scattering. The figure also suggests that with proper inclusion of Coulomb modifications in the theory and/or accurate neutron-deuteron measurements one could actually observe the phenomenological effects due to this $3NF$-like contribution.

We have repeated the same analysis at 8.5 MeV. Figure 5 exhibits that basically the same description found at 3 MeV holds also at this energy. The $3NF$ mechanism under scrutiny is capable to raise the neutron-deuteron A_y in order to match the experimental data without any sen-

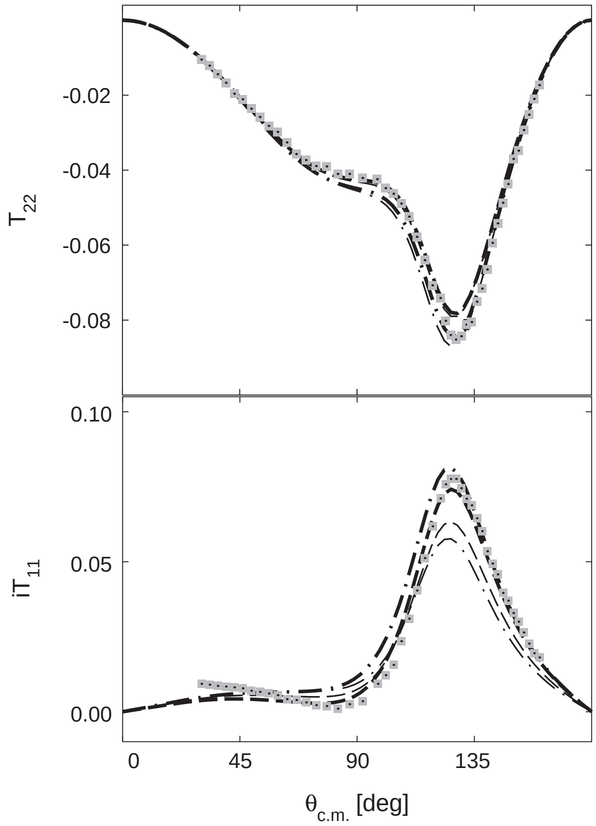

Fig. 6. Same as in fig. 3, but for *nd* scattering at 8.3 MeV. Data are for *pd* scattering at 9 MeV, from ref. [49]. Thick (thin) lines are calculations with (without) inclusion of the irreducible pionic effects, as discussed in this work. The calculations are for the CD-Bonn (dashed lines) and Bonn-B (dot-dashed lines).

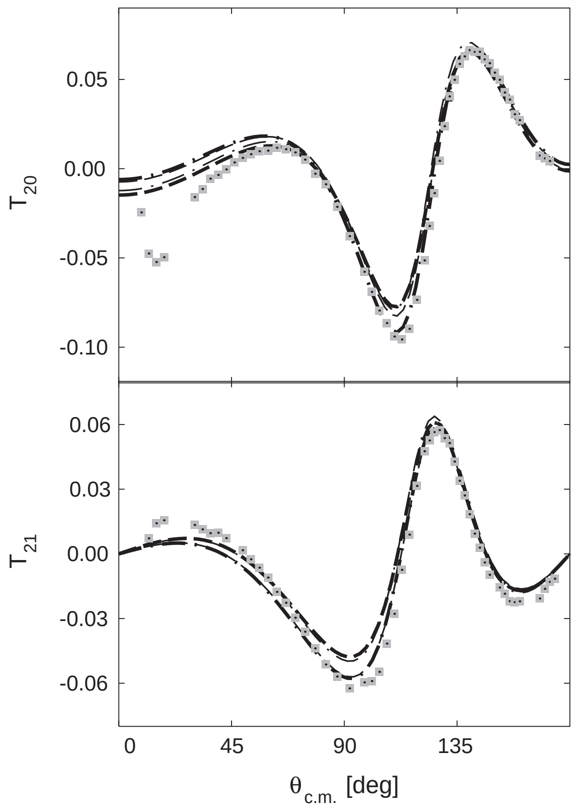

Fig. 7. Same as in fig. 6, but for the T_{20} and T_{21} analyzing powers.

sible modification of the corresponding differential cross-section. As a minor effect, also at this energy we can observe a reduction of the cross-section in the forward and backward directions, for both Bonn-B and CD-Bonn potentials, but in both cases the effect is hardly perceptible in the figure. The cross-section data have been extracted from ref. [47] (open circles) and ref. [42] (open triangles) while the polarization data have been taken from ref. [48].

In figs. 6 and 7 we have compared *nd* theoretical results with *pd* data for the deuteron analyzing powers. For the reasons explained above, we compared results obtained at 8.3 MeV (for incident-neutron energy) with data taken at 18 MeV (incident deuterons) [49]. The lower panel of fig. 6 shows that when including the $3NF$ effect the increase of iT_{11} is about of the right size for both potentials; however, one observes also an inversion of the peaks, since, when including the $3NF$ effect, the Bonn-B peak is higher than the CD-Bonn one, while without $3NF$ the CD-Bonn peak is higher. The same thing was occurring also at lower energy.

For the deuteron tensor analyzing powers, T_{22} (upper panel of fig. 6), T_{20} and T_{21} (upper and lower panels of fig. 7, respectively), we observe that the overall shape of the angular distributions is better reproduced than at 4 MeV, indicating that the effects of Coulomb distortions are less important here (with the exception of the data in the forward direction), and that the modifications introduced by the $3NF$ effects are in general of minor importance with respect to those observed for the vector analyzing powers. A closer inspection, however, reveals that while the OPE-$3NF$ effects are very small for T_{22} for both CD-Bonn and Bonn-B potentials, the situation is different for the other two deuteron tensor observables, where the effects of this $3NF$ diagram can indeed be observed and are about of the same size of the difference between the two potentials themselves. For T_{20} in particular, the $3NF$ effect provides a remarkable improvement of the dip at $110°$ in the case of the Bonn-B potential, while for the case of the CD-Bonn potential the situation is basically unchanged. For T_{21} again the $3NF$ effect remarkably improves the description in the Bonn-B case (especially at the dip around $90°$), while for the case of the CD-Bonn potential the situation is reversed.

Then, we have considered how the situation evolves at 12 MeV. Again we find that the introduction of these irreducible pionic effects are able to increase significantly A_y (lower panel of fig. 8) for both potentials without affecting appreciably the differential cross-section (upper panel of fig. 8). As the energy increases, it becomes evident that the introduction of these $3NF$-like effects provide a good description of A_y in both hemispheres. To obtain this, the corrections have to operate differently in the two directions, with a substantial increase of the analyzing power in the backward hemisphere, where the peak evolves, and

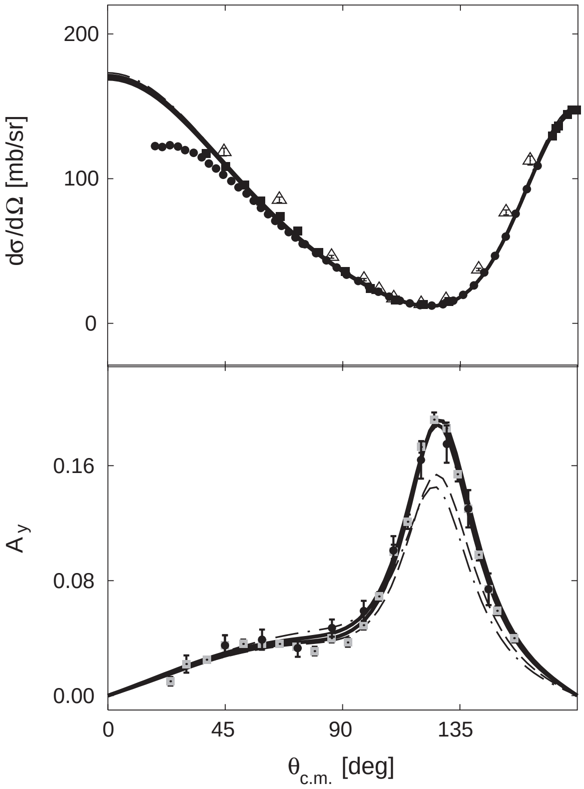

Fig. 8. Same as in fig. 5 but for nucleon scattering at 12.0 MeV. Data for the differential cross-section are from refs. [42] (triangles, *nd*), [50] (circles, *pd*), and [51] (squares, *pd*). Data for the neutron analyzing power (A_y) are from refs. [52] (black circles) and [53] (gray squares). Calculations are for CD-Bonn (dashed line) and Bonn-B (dash-dotted line) potentials. The thick solid line includes the irreducible $3NF$-like effects for both potentials.

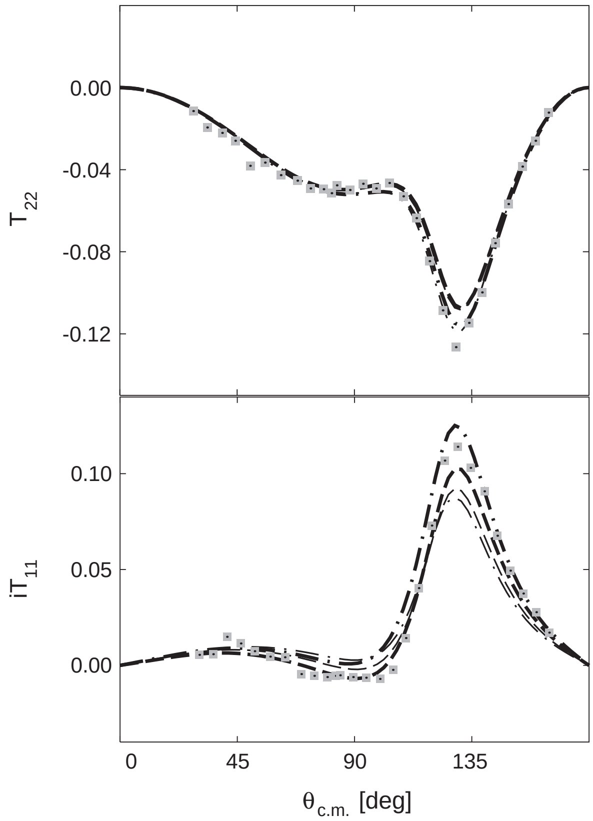

Fig. 9. Same as in fig. 6, but for *nd* scattering at 11.3 MeV. Data are for *pd* scattering at 12 MeV, from ref. [54]. Thick (thin) lines are calculations with (without) inclusion of the irreducible pionic effects, as discussed in this work. The calculations are for the CD-Bonn (dashed lines) and Bonn-B (dot-dashed lines).

at the same time with a slight suppression of A_y in the forward hemisphere, especially for the Bonn-B potential. Clearly, these irreducible pionic effects have the ability to achieve both goals. In figs. 9 and 10 we compare *pd* data measured at the proton-equivalent energy of 12 MeV with *nd* calculations at 11.3 MeV (for consistency with the Coulomb slow-down assumption). For both potentials, the $3NF$-like effects increase iT_{11} significantly in the backward hemishere and suppress slightly the observable at forward angles. Comparison with experimental data suggest that these modifications are correct in both directions, although great caution has to be exercised when comparing *nd* calculation with *pd* data. Around the peak at backward angles we observe also a quite large increase for the case of the Bonn-B potential, while the effect is smaller for the CD-Bonn case. This last feature is similar to what has been observed at lower energy.

The $3NF$-like effects have a very minor impact on T_{22}, also at 12 MeV (upper panel of fig. 9), while it is evident that this observable is more sensitive to the choice of the underlying $2N$ potential, and in absence of other additional contributions, we might conclude that the data seem to favor more the BB-EST calculation, with respect to the CDB-EST results.

In fig. 10 we consider the remaining two tensor analyzing powers, T_{20} (upper panel) and T_{21} (lower panel). T_{20} exhibits an interesting evolution since the results for the BB-EST + OPE-$3NF$ case are significantly different around 110° than the other cases, and they are remarkably close to the experimental data. An interesting situation occurs also for T_{21} around 100°, where the Bonn-B + OPE-$3NF$ calculation are appreciably more negative than the other calculations considered in the figure. We calculated that this same situation evolves also at higher energies (*e.g.*, 18–20 MeV). Unfortunately, no experimental data have been found for T_{21} in this energy range, and new measurements for T_{21} would be very useful in the range of 10–20 MeV.

As has been explained in ref. [18], one basic aspect of the irreducible pionic effects which generate the $3NF$ diagram included in our calculation develops as a consequence of an “imperfect” cancellation with respect to the mesonic retardation contributions. Since in our study we employ realistic nucleon-nucleon potentials, we observe that they are heavily based on fitting procedures of experimental nucleon-nucleon data and are therefore a sort of “black boxes” with respect to the variety and structure of the meson exchange diagrams included, except probably

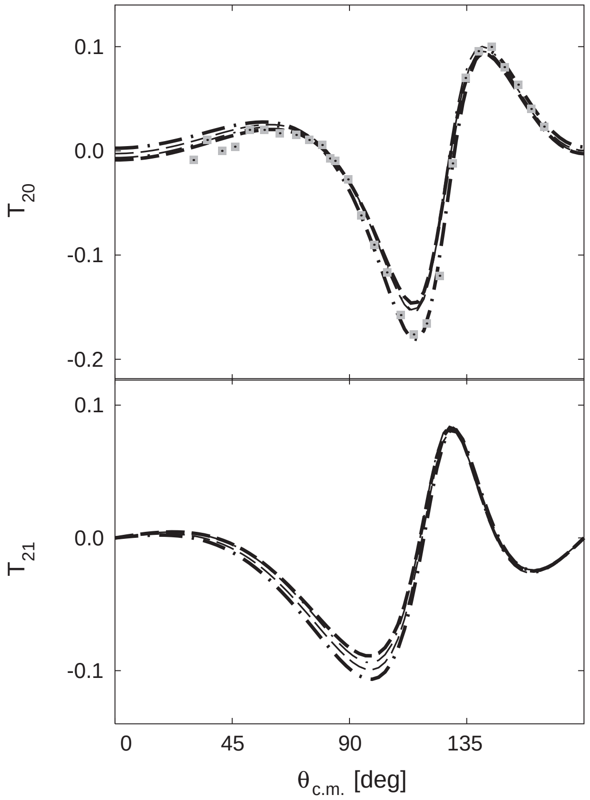

Fig. 10. Same as in fig. 9, but for the T_{20} and T_{21} analyzing powers.

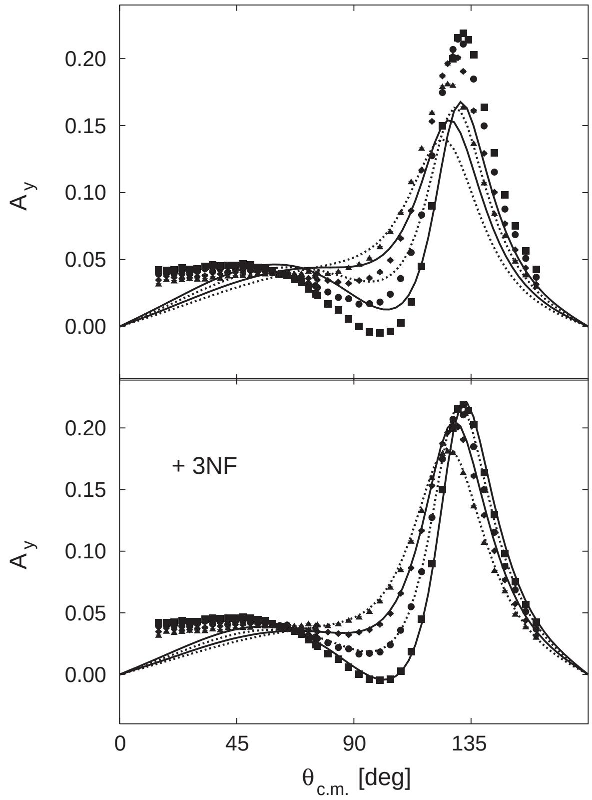

Fig. 11. Evolution of the analyzing power A_y in the range 12–18 MeV. Squares, circles, diamonds and triangles represents *pd* data at 18, 16, 14 and 12 MeV, respectively, taken from ref. [50]. The lines in the upper panel refer to corresponding calculations with the Bonn-B potential, while in the lower panel the OPE-$3NF$ effects are also included.

the OPE term, since only the longest range of the nuclear force is well established. It should therefore not be a surprise that for each $2N$ potential we included in the corresponding $3NF$ diagram a phenomenological parameter that governs the level of cancellation against meson retardation effects. In the approach we developed in ref. [19] we used the experimental value of A_y at the peak to actually fix this parameter. Then, it is obviously of interest to study how this parameter evolves with energy. For this reason we considered the wealth of *pd* experimental data for A_y measured at 12, 14, 16, and 18 MeV (ref. [50]) and compared these data with *nd* calculations at 11.3, 13.3, 15.3, and 17.3 MeV, respectively, finding that we could reproduce how the peak evolves with a perfectly linear dependence of the parameter governing the cancellation of the $3NF$.

The situation is shown in figs. 11 and 12 for the Bonn-B and CD-Bonn potentials. In the two figures, the upper panel compares data with results taken without $3NF$, while the results in the lower panel include the $3NF$ effect. Inclusion of the OPE-$3NF$ effect provides very good results for the Bonn-B potential, not only in the region of the peak (around 130° MeV), but also in the region around 100° where the dip evolves. For the CD-Bonn potential the situation is similarly satisfactorily for the evolution of the A_y peak while the evolution of the dip at lower angles is fair but not optimal. For both potentials, we report in table 2 the value of the parameter and the corresponding energy we have employed in calculating this $3NF$ effect.

In this same energy range, we focus attention on the nucleon-deuteron polarization transfer coefficients, $K_y^{y'}$, $K_z^{x'}$, $K_y^{x'x'-y'y'}$, and $K_y^{z'z'}$. It has been suggested in ref. [55] that these observables are sensitive to the tensor part of the nuclear forces and therefore they could in principle represent a good testing ground for the $3NF$-operator we are studying in the present paper, since this has a pronounced tensor structure. In addition, experimental data are now available, for both *nd* and *pd* systems, and a number of theoretical studies about these coefficients have been performed already [51,55–58] with a variety of different $2N$ potentials, with the addition of $3NF$'s, and more recently also with the inclusion of the modifications introduced by Coulomb effects. From these studies it emerged that the nucleon-to-nucleon transfer coefficients $K_y^{y'}$ and $K_z^{x'}$ exhibit a scaling behavior with respect to the triton binding energy, while the nucleon-to-deuteron coefficients $K_y^{x'x'-y'y'}$, and $K_y^{z'z'}$ do not scale. Moreover, $K_y^{y'}$ and $K_z^{x'}$ exhibit sizable Coulomb effects, while for the other two coefficients the effects are much less appreciable. For the case of $K_y^{y'}$, where it was possible to compare directly theory with *nd* data, it was found that the theoretical calculations underpredict the minimum at 110°, once the scaling effect with binding, originated by the 2π

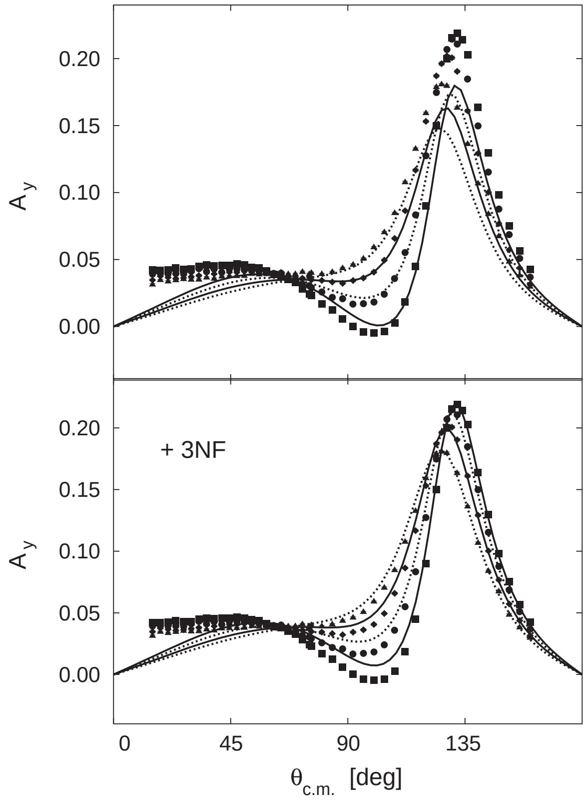

Fig. 12. Same as in fig. 11 but for the CD-Bonn potential.

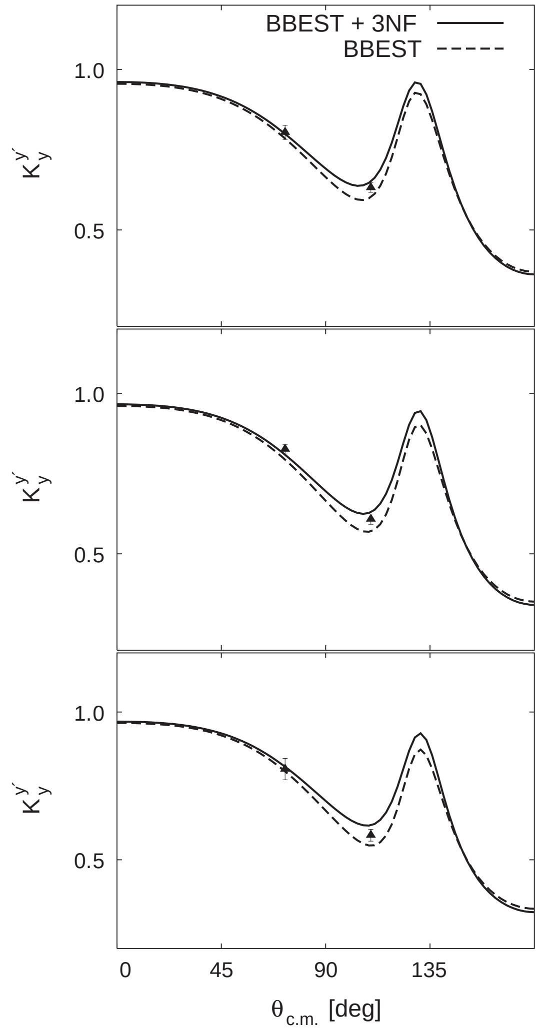

Fig. 13. Spin transfer coefficient $K_y^{y'}$ at 15 MeV (upper panel), 17 MeV (middle panel), and 19 MeV (lower panel). Comparison between nd data from ref. [56] and Bonn-B calculations. Solid (dashed) lines include (exclude) the irreducible $3NF$-like pionic effects.

exchange $3NF$, was properly taken into account. Moreover, discrepancies between theoretical calculations and experimental data concerning the Coulomb effects for $K_y^{y'}$ at 19 MeV suggest that the situation is not fully understood. For the nucleon-to-deuteron tensor transfer coefficients the situation is also unclear, since Coulomb effects and traditional 2π exchange $3NF$ provide too small modifications for a correct reproduction of data (for $K_y^{x'x'-y'y'}$ the peak at 135° is underestimated). This state of affairs demands for more theoretical investigations; at the same time more extensive experimental studies for these observables in this energy range could be extremely useful.

In figs. 13 and 14 we show the results obtained with the Bonn-B and CD-Bonn potentials, respectively, and compare these with experimental nd data taken at 15, 17, and 19 MeV, ref. [56]. Our calculations do not include the effects of the 2π exchange $3NF$, and therefore one should take into account in the discussion the rescaling effect that tend to push the lines downward (this tendency is however reduced with the Bonn-types interactions, which provide smaller $3N$ underbinding with respect to other $2N$ interactions). The results for the Bonn-B case suggest that the $3NF$ effect we have calculated is able to correct the underprediction of the minimum of $K_y^{y'}$ at 110°, however the results with the CD-Bonn potential do not confirm this indication, since the modifications are smaller here and have the tendency to go in the opposite direction. In figs. 15 and 16 we similarly compare the pd data at 19 MeV [55] with nd calculations at 18.3 MeV. This comparison has to be made with great caution, since Coulomb effects and the 2π-$3NF$ provide appreciable effects, but the two modifications tend somewhat to cancel out [57]. Nevertheless, it is interesting to observe that here the minimum of $K_y^{y'}$ is appreciably overpredicted in the Bonn-B case (lower panel of fig. 15) while in the case of the CD-Bonn potential the irreducible pionic effects do not affect the results appreciably and therefore they maintain the quality of the fit (lower panel of fig. 16). Thus, the experimental "mismatch" between the nd and pd data for $K_y^{y'}$ at 19 MeV acquires an interesting twist: the nd data seem to support the Bonn-B + OPE-$3NF$ calculations, the pd data seem to support more the CD-Bonn + OPE-$3NF$ results.

Finally, in figs. 17 and 18 the tensor transfer coefficients are compared with experiments [58] at 19 MeV. Again, we observe appreciable effects introduced by the OPE-$3NF$ diagram in the case of the Bonn-B interaction, while for the CD-Bonn case the effects appear to

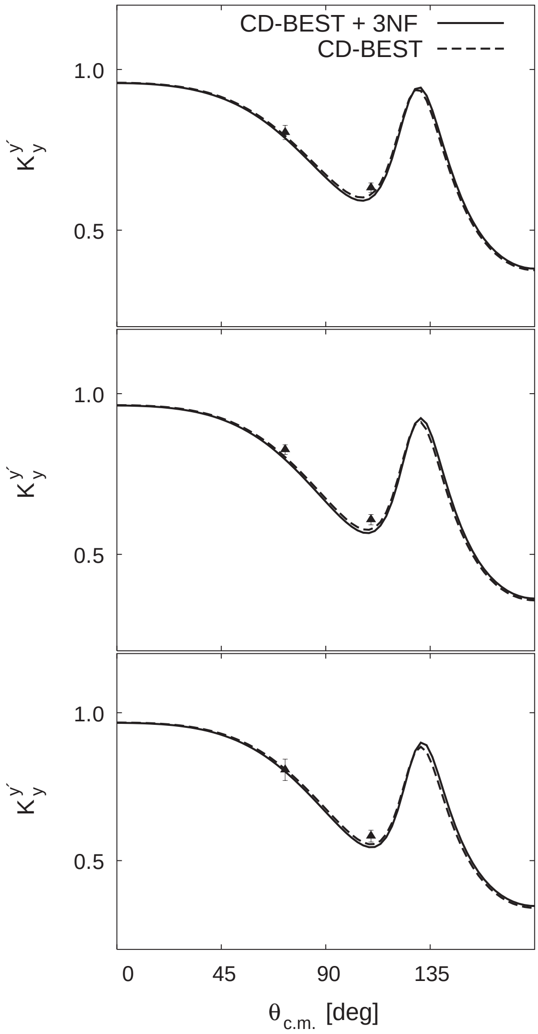

Fig. 14. Same as in fig. 13 but for the CD-Bonn potential.

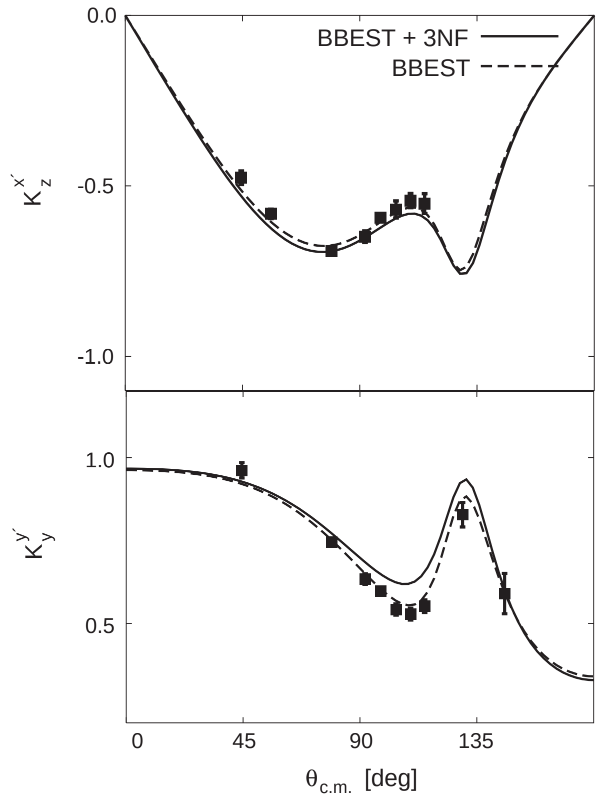

Fig. 15. Calculations for the nd spin transfer coefficients $K_z^{x'}$ (upper panel) and $K_y^{y'}$ (lower panel), at 18.3 MeV, for the Bonn-B potential. Data are for the equivalent pd observables at 19.0 MeV, from ref. [55]. Solid (dashed) lines include (exclude) the irreducible $3NF$-like pionic effects.

be smaller, although they go in the same direction. We observe that the calculation with Bonn-B + OPE-$3NF$ (fig. 17) is able to solve the underprediction problem in $K_y^{x'x'-y'y'}$, but at the same time it increases the discrepancies in $K_y^{z'z'}$, while in the case of the CD-Bonn + OPE-$3NF$ the situation remains essentially unchanged (fig. 18).

4 Conclusions

We have studied the low-energy effects in nucleon-deuteron scattering due to an irreducible pionic effect leading to a $3NF$ diagram of pronounced tensor structure. Overall we find that the effects of this diagram on the differential cross-section are negligible in the considered energy range, indicating that the average impact of this $3NF$ diagram on $3N$ dynamics is small. On the other hand, for the case of the spin observables, the higher sensitivity to the smaller components of the wave function is able to detect the presence of this contribution. This is so especially for the case of the vector analyzing powers A_y and iT_{11}, which are considered to be a magnifying glass for the triplet P waves of the $2N$ subsystem. Independently of the $2N$ interactions used as input, we found that this $3NF$ contribution has the potential to significantly increase (about a 30% effect) the magnitude of these two observables, and to solve a discrepancy observed long time ago. This is a consequence of the specific spin-isospin structure of such $3NF$ diagram which affects in a privileged manner the triplet odd states [18,19].

For the remaining spin observables (tensor analyzing powers and polarization transfer coefficients) the changes due to this pionic contribution are small, however we found situations where the diagram produces appreciable effects. In particular with the use of the Bonn-B potential there are indications that the corrections produced move towards the right direction, but the results with the newer CD-Bonn potential reduce the size of these changes considerably. We found few cases where the calculations are slightly —but appreciably— different when the $3NF$ effect is calculated with Bonn-B or CD-Bonn potentials. It happens with T_{21} in the energy range 10–20 MeV, with $K_y^{y'}$ in the energy range 15–19 MeV, and with $K_y^{x'x'-y'y'}$ and $K_y^{z'z'}$ around 19 MeV. There are however still too many uncertainties for arriving at a definite conclusion about these slight differences. Comparison of the wealth of

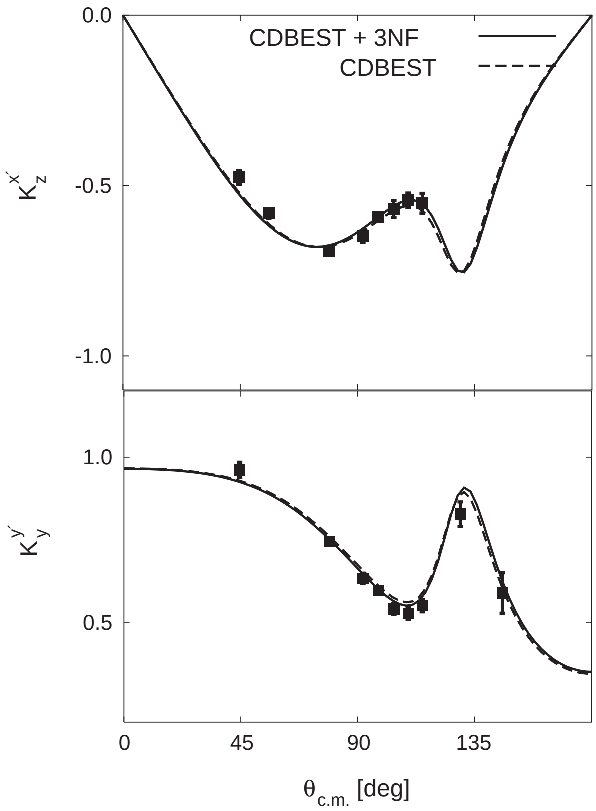

Fig. 16. Same as in fig. 15 but for the CD-Bonn potential.

experimental data for charged particles has been done using only the Coulomb slow-down hypothesis, while a consistent inclusion of Coulomb effects is in principle required. Finally, a more complete study requires also the inclusion of the remaining $3NF$ diagrams of different topology. In particular, it is known that the 2π-$3NF$ diagram produces additional corrections which are needed for removing the underbinding of the $3N$ bound state. The influence on the vector analyzing powers in the considered energy range, however, appears to be marginal.

This work is supported by the Italian MURST-PRIN Project "Fisica Teorica del Nucleo e dei Sistemi a Più Corpi". W.S. thanks INFN and the University of Padova for hospitality and acknowledges support from the Natural Science and Engineering Research Council of Canada.

Appendix A. Binding energy

With the same model interactions used in the main text, we have calculated also the triton binding energy. The results are given in table 3. For each one of the three potentials, the first value in the table reports the $3N$ binding energy calculated by a direct solution of the homogeneous Faddeev equation in two momentum variables (2D), using the original $2N$ potential as input, and without resorting to the separable expansion method. Details on the computational method are explained in ref. [41] and refer-

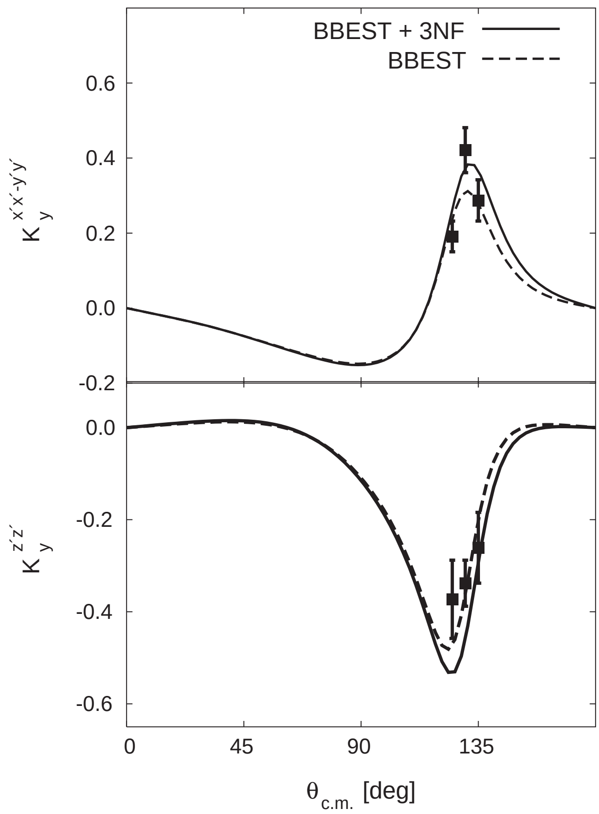

Fig. 17. Polarization transfer coefficients $K_y^{x'x'-y'y'}$ (top) and $K_y^{z'z'}$ (bottom) calculated at 18.3 MeV for the Bonn-B potential. Data are for pd scattering at 19.0 MeV, from [58].

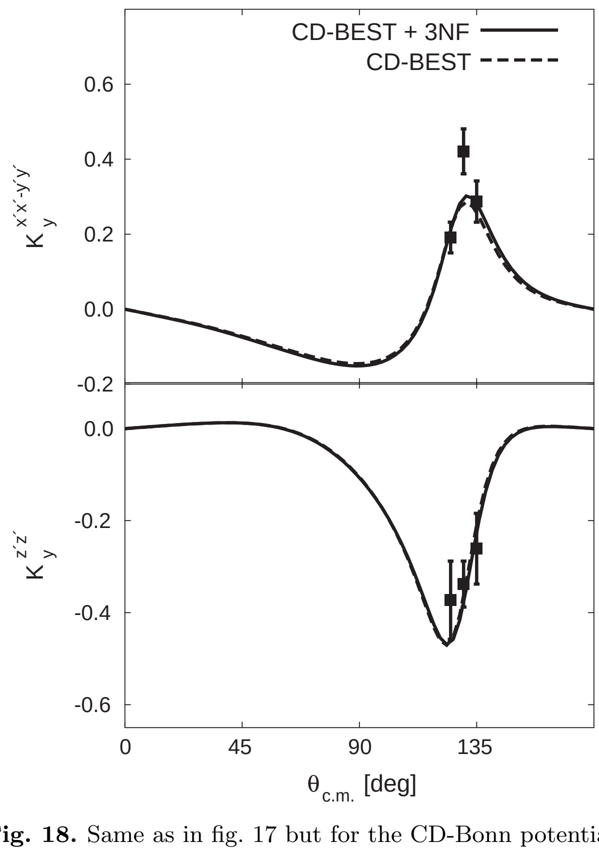

Fig. 18. Same as in fig. 17 but for the CD-Bonn potential.

Table 3. Results obtained for the triton binding energy (MeV). The first three lines correspond to different calculational methods without the inclusion of the $3NF$ effect. The last line includes the effects of the OPE-$3NF$ diagram. The $3NF$ effect has been calculated with the effective parameter c determined at 3 MeV.

	Paris	Bonn-B	CD-Bonn
2D − orig	−7.385	−8.101	−7.958
2D − EST	−7.376	−8.088	−7.947
1D − EST	−7.376	−8.088	−7.947
1D + $3NF$	−7.663	−7.943	−8.077

ences therein. The second value has been calculated also via a direct solution of the 2D Faddeev equation, but this time using as input the separable expansion of the $2N$ potential, with the same ranks as given in table 1. The third value represents the binding energy obtained with the same separable representation of the $2N$ potential as in the previous line, but using the one-dimensional algorithm corresponding to the Lovelace-Alt-Grassberger-Sandhas homogeneous equation [41]. Finally, the last line includes the irreducible pionic effects, as discussed in this work, in the 1D calculation for the binding energy.

References

1. W. Glöckle, P.U. Sauer, Europhys. News **15-2**, 5 (1984).
2. P.U. Sauer, Nucl. Phys. A **543**, 291 (1992).
3. J.L. Friar, S.A. Coon, Phys. Rev. C **49**, 1272 (1994)
4. A.W. Thomas, A.S. Rinat, Phys. Rev. C **20**, 216 (1979); I.R. Afnan, B. Blankleider, Phys. Rev. C **22**, 1638 (1980); **32**, 2006 (1985); Y. Avishai, T. Mizutani, Nucl. Phys. A **326**, 352 (1979); **338**, 377 (1980); **352**, 399 (1981); Phys. Rev. C **27**, 312 (1983).
5. H. Garcilazo, T. Mizutani, *πNN Systems* (World Scientific, Singapore, 1990).
6. L. Canton, Phys. Rev. C **58**, 3121 (1998).
7. O.A. Yakubovskĭ, Yad. Fiz. **5**, 1312 (1967) (English version: Sov. J. Nucl. Phys. **5**, 937 (1967)).
8. P. Grassberger, W. Sandhas, Nucl. Phys. B **2**, 181 (1967).
9. Y. Avishai, T. Mizutani, Nucl. Phys. A **393**, 429 (1983).
10. G. Cattapan, L. Canton, J.P. Svenne, Nuovo Cimento A **106**, 1229 (1993).
11. L. Canton, G. Cattapan, Phys. Rev. C **50**, 2761 (1994); G. Cattapan, L. Canton, Few-Body Syst. **17**, 163 (1994); Phys. Rev C **56**, 689 (1997).
12. L. Canton, T. Melde, J.P. Svenne, Phys. Rev. C **63**, 034004 (2001).
13. E.O. Alt, P. Grassberger, W. Sandhas, Nucl. Phys. B **2**, 167 (1967).
14. S. Weinberg, Phys. Lett. B **295**, 114 (1992).
15. S.A. Coon, M.D. Scadron, P.C. McNamee, B.R. Barrett, D.W.E. Blatt, B.H.J. McKellar, Nucl. Phys. A **317**, 242 (1979).
16. H.T. Coelho, T.K. Das, M.R. Robilotta, Phys. Rev. C **28**, 1812 (1983); M.R. Robilotta, H.T. Coelho, Nucl. Phys. A **460**, 645 (1986).
17. H. Haberzettl, W.C. Parke, in *Few-Body Problems in Physis*, edited by F. Gross (Williamsburg, VA, 1994); *AIP Conf. Proc.* Vol. **334** (AIP, New York, 1995) p. 871.
18. L. Canton, W. Schadow, Phys. Rev. C **62**, 044005 (2000).
19. L. Canton, W. Schadow, Phys. Rev. C **64**, 031001(R) (2001).
20. L. Canton, G. Pisent, W. Schadow, T. Melde, J.P. Svenne, in *Theoretical Nuclear Physics in Italy, Proceedings of the 8th Conference on Problems in Theoretical Nuclear Physics, Cortona, Italy, October 18-20*, edited by G. Pisent, S. Boffi, L. Canton, A. Covello, A. Fabrocini, S. Rosati (World Scientific, Singapore, 2001) p. 249.
21. S.Y. Yang, W. Glöckle, Phys. Rev. C **33**, 1774 (1986).
22. S.A. Coon, J.L. Friar, Phys. Rev. C **34**, 1060 (1986).
23. E. Epelbaoum, W. Glöckle, Ulf-G. Meißner, Nucl. Phys. A **637**, 107 (1998).
24. S.M. Coon, M.T. Peña, D.O. Riska, Phys. Rev. C **52**, 2925 (1995).
25. D. Hüber, J.L. Friar, A. Nogga, H. Witała, U. van Kolck, Few-Body Syst. **30**, 95 (2001).
26. A. Kievsky, Phys. Rev. C **60**, 034001 (1999).
27. F. Sammarruca, H. Witała, X. Meng, Acta Phys. Pol. B **31**, 2039 (2000).
28. G.E. Brown, N. Rho, Phys. Rev. Lett. **66**, 2720 (1991).
29. W. Tornow, H. Witała, Nucl. Phys. A **637**, 280 (1998).
30. D. Hüber, J.L. Friar, Phys. Rev. C **58**, 674 (1998).
31. R. Machleidt, Phys. Rev. C **63**, 024001 (2001).
32. V. Stoks, R. Timmerman, J.J. de Swart, Phys. Rev. C **49**, 2729 (1994).
33. R.A. Arndt, I.I. Strakovsky, R.L. Workman, M.M. Pavan, Phys. Rev. C **52**, 2120 (1995).
34. Y. Koike, J. Haidenbauer, Nucl. Phys. A **463**, 365c (1987).
35. Y. Koike, J. Haidenbauer, W. Plessas, Phys. Rev. C **35**, 1588 (1987).
36. J. Haidenbauer, unpublished.
37. L. Lacombe, B. Loiseau, J.M. Richard, R. Vinh Mau, J. Coté, P. Pirès, R. de Tourreil, Phys. Rev. C **21**, 861 (1980).
38. R. Machleidt, K. Holinde, Ch. Elster, Phys. Rep. **149**, 1 (1987); R. Machleidt, Adv. Nucl. Phys. **19**, 189 (1989).
39. D.J. Ernst, C.M. Shakin, R.M. Thaler, Phys. Rev. C **8**, 46 (1973).
40. T. Cornelius, W. Glöckle, J. Haidenbauer, Y. Koike, W. Plessas, H. Witała, Phys. Rev. C **41**, 2538 (1990).
41. W. Schadow, W. Sandhas, J. Haidenbauer, A. Nogga, Few-Body Syst. **28**, 241 (2000).
42. P. Schwarz, H.O. Klages, P. Doll, B. Haesner, J. Wilczynski, B. Zeitnitz, J. Kecskementi, Nucl. Phys. A **398**, 1 (1983).
43. J.E. McAninch, L.O. Lamm, W. Haeberli, Phys. Rev. C **50**, 589 (1994).
44. S. Shimizu, K. Sagara, H. Nakamura, K. Maeda, T. Miwa, N. Nishimori, S. Ueno, T. Nakashima, S. Morinobu, Phys. Rev. C **52**, 1193 (1995).
45. W. Tornow, C.R. Howell, R.L. Walter, I. Šlaus, Phys. Rev. C **45**, 459 (1992).
46. A. Kievsky, M. Viviani, S. Rosati, Phys. Rev. C **64**, 024002 (2001).
47. T. Hongquin, Y. Chunying, S. Guanren, L. Anli, H. Tangzi, Chin. J. Nucl. Phys. **8**, 50 (1986).
48. W. Tornow, C.R. Howell, M. Al Ohali, Z.P. Chen, P.D. Felsher, J.M. Hanly, R.L. Walter, G. Weisel, G. Mertens, I. Slaus, H. Witała, W. Glöckle, Phys. Lett. B, **257**, 273 (1991).

49. K. Sagara, private communication.
50. K. Sagara, H. Oguri, S. Shimizu, K. Maeda, H. Nakamura, T. Nakashima, S. Morinobu, Phys. Rev. C **50**, 577 (1994).
51. G. Rauprich, H.J. Hähn, M. Karus, P. Niessen, K.R. Nyga, H. Oswald, L. Sydow, H. Paetz gen. Schieck, Y. Koike, Few-Body Syst. **5**, 67 (1988).
52. W. Tornow, P.W. Lisowski, R.C. Byrd, R.L. Walter, Nucl. Phys. A **296**, 23 (1978).
53. W. Tornow, C.R. Howell, R.L. Walter, Nucl. Instrum. Methods B **40**, 470 (1989).
54. W. Grüebler, V. König, P.A. Schmelzbach, F. Sperisen, B. Jenny, R.E. White, F. Seiler, H.W. Roser, Nucl. Phys. A **398**, 445 (1983).
55. L. Sydow, S. Lemaître, P. Niessen, K.R. Nyga, G. Rauprich, R. Reckenfelderbaümer, S. Vöhl, H. Paetz gen. Schieck, H. Witała, W. Glöckle, Nucl. Phys. A **567**, 55 (1994).
56. P. Hempen, P. Clotten, K. Hofenbitzer, T. Kölbe, W. Metschulat, M. Schwindt, W. von Witsch, L. Wätzold, J. Welts, W. Glöckle, D. Hüber, Witała, Phys. Rev. C **57**, 484 (1998).
57. A. Kievsky, S. Rosati, M. Viviani, Phys. Rev. C **64**, 041001 (2001).
58. L. Sydow, S. Vöhl, S. Lemaître, H. Patberg, R. Reckenfelderbaümer, H. Paetz gen. Schieck, W. Glöckle, D. Hüber, H. Witała, Few-Body Syst. **25**, 133 (1998).